Marine Pollution Bulletin 216 (2025) 118005

Contents lists available at ScienceDirect

Marine Pollution Bulletin

journal homepage: www.elsevier.com/locate/marpolbul

Experimental study of buoyant macro- and mesoplastic trapping by *Spartina maritima*

Paula Núñez [a,*], Laura Pérez-García [a], Seyed Meysam Rezaee [b], Javier F. Bárcena [a], Andrés García [a]

[a] IHCantabria - Instituto de Hidráulica Ambiental de la Universidad de Cantabria, Santander, Spain
[b] AIMS - The Australian Institute of Marine Science, Darwin, Australia

ARTICLE INFO

Keywords:
Macro−/mesoplastics
Plastic debris trapping
Spartina maritima
Estuaries
Salt marshes
Laboratory experiments

ABSTRACT

A set of laboratory experiments was conducted to assess the trapping efficiency of buoyant plastic debris by the estuarine vegetation *Spartina maritima*. Different hydrodynamic conditions typical of salt marshes were simulated in a hydraulic flume. These conditions included varying water levels between 40% and 90% of stem height, wind speeds up to 2 m/s, and unidirectional current velocities between 0.1 and 0.3 m/s. Moreover, three vegetation densities (small/medium/high) and nine plastic debris types varying in shape (elongated/two-dimensional/three-dimensional) and size (macro/meso) were tested. The results indicate that *Spartina maritima* functions as a natural trap. Specifically, the study highlights that lower surface velocities, higher stem densities, greater emergent heights, and larger debris sizes significantly enhance trapping efficiency. It was also inferred that for a *Spartina maritima* density comparable to that observed in marshes, the dominance of surface velocity or debris size effects on trapping efficiency is primarily dependent on debris shape. Consequently, surface velocity has a greater impact on two-dimensional elements, whereas debris size is more significant for three-dimensional elements. Finally, a preliminary trapping model was developed to integrate all the aforementioned variables. This model has the potential to enhance the accuracy of numerical predictions regarding the transport and fate of plastic debris using Lagrangian modeling, and can be further refined by incorporating additional data.

1. Introduction

The presence of plastic debris in the marine environment is currently a major global concern (Cózar et al., 2014; Galgani et al., 2015; Law, 2017). Macro- (>25 mm), meso- (5–25 mm), and microplastics (<5 mm) pose multiple threats to the health and stability of marine and estuarine ecosystems (Crawford and Quinn, 2017). These primary risks include entanglement, ingestion, and the transport of toxic chemicals attached to their surfaces (Galloway et al., 2017; Kühn and Van Franeker, 2020; Zhao et al., 2024). Hence, the presence of plastic debris in the aquatic environment has also been recognized as a global issue (Díaz-Torres et al., 2017; Meijer et al., 2021), comparable to other global concerns such as climate change, ocean acidification, and loss of biodiversity (Tiller et al., 2019).

Approximately 80% of marine plastics come from land-based sources, mainly from rivers (Rech et al., 2014; Galgani et al., 2015; Lebreton et al., 2017; Tramoy et al., 2020; Meijer et al., 2021). It is estimated that the global river system annually contributes between 1.5 and 2.4 million tons of plastic material to the oceans (Lebreton et al., 2017). As transitional areas between rivers and oceans, estuaries are hotspots for the accumulation of plastic debris before it reaches the ocean (Mazarrasa et al., 2019; Núñez et al., 2019; Yao et al., 2019; Li et al., 2024), where it is transported by waves (Alsina et al., 2020; Forsberg et al., 2020; Kerpen et al., 2020, 2024; Núñez et al., 2023b; Iuppa et al., 2024), wind, and currents to the coast, to the wave breaking zones, or to oceanic convergence gyros (Lebreton et al., 2012; Maximenko et al., 2012; Van Sebille et al., 2012, 2020). Therefore, understanding the trapping role of estuarine areas is crucial for developing effective mitigation and cleanup strategies, ultimately reducing the entry of plastic debris into the ocean.

The transport, dispersion, and trapping of plastic debris in estuaries are significantly influenced by the interactions between tidal and fluvial currents, wind forces, and the presence of salt marshes (Jalón-Rojas et al., 2019; Núñez et al., 2019, 2020, 2021; Li et al., 2024). Salt marshes are tidal flats that host a wide variety of estuarine vegetal species,

* Corresponding author.
E-mail address: nunezp@unican.es (P. Núñez).

https://doi.org/10.1016/j.marpolbul.2025.118005
Received 17 December 2024; Received in revised form 31 March 2025; Accepted 15 April 2025
Available online 19 April 2025

including *Spartina* spp., *Halimione* spp., *and Juncus* spp., among others. These vegetated communities reduce flow velocities and inhibit both offshore and onshore transport during tidal cycles (Zhao et al., 2015; Mazarrasa et al., 2019, 2023; Yao et al., 2019; Wu et al., 2020; Cesarini and Scalici, 2022; Ogbuagu et al., 2022; Girones et al., 2024). Consequently, salt marshes function as natural barriers that promote the accumulation of plastic debris, particularly macro- and meso-sized particles. These particles are more readily trapped and subsequently degraded and transformed into microplastics within these areas (Yao et al., 2019; Cozzolino et al., 2020; Newbould et al., 2021; Cesarini and Scalici, 2022).

Previous field studies have demonstrated a direct correlation between the presence of estuarine vegetation and the ability of estuaries to trap plastic debris. These studies analyzed the trapping efficiency across different vegetation communities located in intertidal zones, namely: *Spartina* spp. (Mazarrasa et al., 2019; Yao et al., 2019; Cozzolino et al., 2020; Almeida et al., 2023; Girones et al., 2024), *Juncus* spp. (Mazarrasa et al., 2019; Almeida et al., 2023), *Halimione* spp. (Mazarrasa et al., 2019), *Zostera noltii* (Cozzolino et al., 2020), *Phragmites australis* (Almeida et al., 2023), and *Sarcocornia perennis* (Girones et al., 2024). Moreover, the most common types of plastic debris found in these locations were also documented. In general, the studies found that high-marsh communities (e.g., *Juncus* spp. or *Halimione* spp.) exhibited higher concentrations of plastic debris compared to adjacent low-marsh communities (e.g., *Spartina* spp.). However, the underlying causes remain unclear because these studies did not investigate the potential relationship between trapping efficiency and hydrodynamic conditions. Therefore, it is uncertain whether the observed differences are attributable to vegetation characteristics or to variations in flooding- ebbing processes between the two marsh areas.

Numerical models have mainly focused on analyzing the influence of plastic sources, hydrodynamics, and wind drag on the dispersion, trapping, and hotspot formation of plastic debris in estuarine environments (Jalón-Rojas et al., 2019; Núñez et al., 2019, 2021; López et al., 2021; Chen et al., 2023; García-Rellán et al., 2023; Li et al., 2024). Nevertheless, these models often do not consider the influence of vegetation, mainly due to the lack of necessary information linking trapping to hydrodynamics, vegetation, and plastic debris characteristics. As suggested by some conceptual models (Vermeiren et al., 2016; Liro et al., 2020) and review studies (Lechthaler et al., 2020; García-Rellán et al., 2023), there remains a significant knowledge gap in this area, necessitating laboratory studies to address it.

Some laboratory experiments have begun to investigate how hydrodynamics, vegetation characteristics (distribution, morphology, and density), and plastic debris properties influence trapping (de Los Santos et al., 2021; Ogbuagu et al., 2022; Gallitelli et al., 2023). These studies analyzed species such as *Spartina anglica, Zoostera noltii*, or lagoon communities, among others. The results suggest that, in addition to vegetation density, the density and size of plastic debris are among the most important factors influencing trapping. Macro- and mesoplastic debris are more likely to be trapped than microplastics, and non-buoyant microplastics are more prone to entrapment than buoyant microplastics, even at high current velocities. Despite these findings, further complementary research is required to gain insights into the complex interactions between the many factors involved.

This study aims to evaluate the efficiency of estuarine vegetation *Spartina maritima* in trapping buoyant macro- and mesoplastic debris. To this end, a series of laboratory experiments were conducted in a hydraulic flume, considering a wide range of shapes and sizes of buoyant macro- and mesoplastics under a range of hydrodynamic conditions representative of salt marshes. As a result, a database was developed, and an expression was derived that relates the trapping of *Spartina maritima* to the shape and size of plastic debris and salt marsh currents. This expression can be incorporated into numerical models of plastic debris transport and dispersion to improve their predictive ability to identify plastic debris hotspots in estuaries. Therefore, in line with the goals set by the 2030 Agenda and Sustainable Development Goals (SDGs 6 and 14) (Nations, 2015), the results of this study provide relevant information to assist managers and policymakers in developing effective strategies against plastic pollution.

2. Material and methods

2.1. Experimental setup

The experiments were conducted in the hydraulic flume of the Instituto de Hidráulica Ambiental of the University of Cantabria (IHCantabria, Spain), which comprises three different zones: the hydraulic flume has a length of 12 m, a width of 0.35 m and a height of 0.5 m (Z1); the transition zone is 1.9 m long, 0.35 m wide and has a linearly variable height ranging from 0.5 m to 0.6 m (Z2); and the expansion zone is 4.1 m long, 1.50 m wide, and 0.6 m high, and serves to stabilize the system of currents (Z3). Furthermore, energy dissipators were installed at the flume entrance to mitigate the flow's energy and velocity prior to its entry into the experimental zone. Vegetation was placed in Z1, covering an area of 1 m × 0.26 m at its base, with an average stem height (h) of 0.2 m (Fig. 1a and c).

The hydraulic flume is equipped with a centrifugal pump with a flow capacity of 100 L/s, a rated power of 15 kW, and a rotational speed of 1,450 rpm. The pump is designed to operate at various frequencies up to 50 Hz. A butterfly valve regulates the flow rate into the flume (Fig. 1g). Fig. 1h illustrates the pump performance curve with the valve fully open, derived from the relationship between flow rates and corresponding pump operating frequencies. At the end of the expansion zone, an adjustable discharge gate allows for water level regulation (Fig. 1b). Additionally, an axial-type fan with 38 cm diameter blades, a power of 0.3 kW, and an operational frequency up to 50 Hz generates wind (Fig. 1d). The fan is located 4.5 m from the water inlet and features an adjustable duct to direct the airflow in the same direction as the waterflow. In the experiments, the air duct length was set at 2.5 m, defining the experimental zone between this point and the end of the vegetation. Fig. 1f shows the correlation between fan operating frequencies and the velocity generated at a distance of 3.0 m from the fan and at a height of 0.2 m above the water surface. This figure was obtained from air velocity measurements at different fan operating frequencies and water levels (9, 14.5, and 18.5 cm). Since velocity variations at the same fan frequency were negligible at different vertical positions, the average fan performance curve was plotted.

Twenty-seven (27) hydrodynamic conditions (HC) were replicated through the combination of varying water levels (η), flow rates (Q), and wind speeds (u_w), thereby representing typical current magnitudes observed in salt marshes (Table 1). By varying these parameters, hydrodynamic conditions were controlled, and water level adjustments specifically allowed for examining the effect of emerged stem height ($h_e = h - \eta$) of *Spartina maritima* on trapping (Fig. 1i). Unidirectional flows were analyzed to assess trapping once plastic debris was transported to the vegetation by currents. Free surface elevations were measured with millimeter precision using a graduated scale at positions upstream and downstream of the vegetation to monitor vegetation-induced water level changes. Flow rates were recorded with a flow meter, and currents were recorded with an Acoustic Doppler Velocimeter (ADV) at a sampling rate of 50 Hz. To establish baseline flow conditions, velocity measurements were taken 0.45 m upstream of the vegetated area, where the vegetation's influence was assumed to be minimal. Velocity measurements were conducted at depths from 1.0 to 12.5 cm from the bottom, with the number of measurement points increasing with water level (Fig. 1i). Furthermore, the surface velocity at the ADV location for each HC was estimated by following the trajectories of buoyant plastic items (representing flow tracers) with a video camera. The camera was a high-resolution video camera (4 MP Fixed Bullet Network Cameras, HIKVISION) with a 4 mm lens, a resolution of 2560 × 1440 pixels, and a frame rate of 20 fps. This camera was placed at a

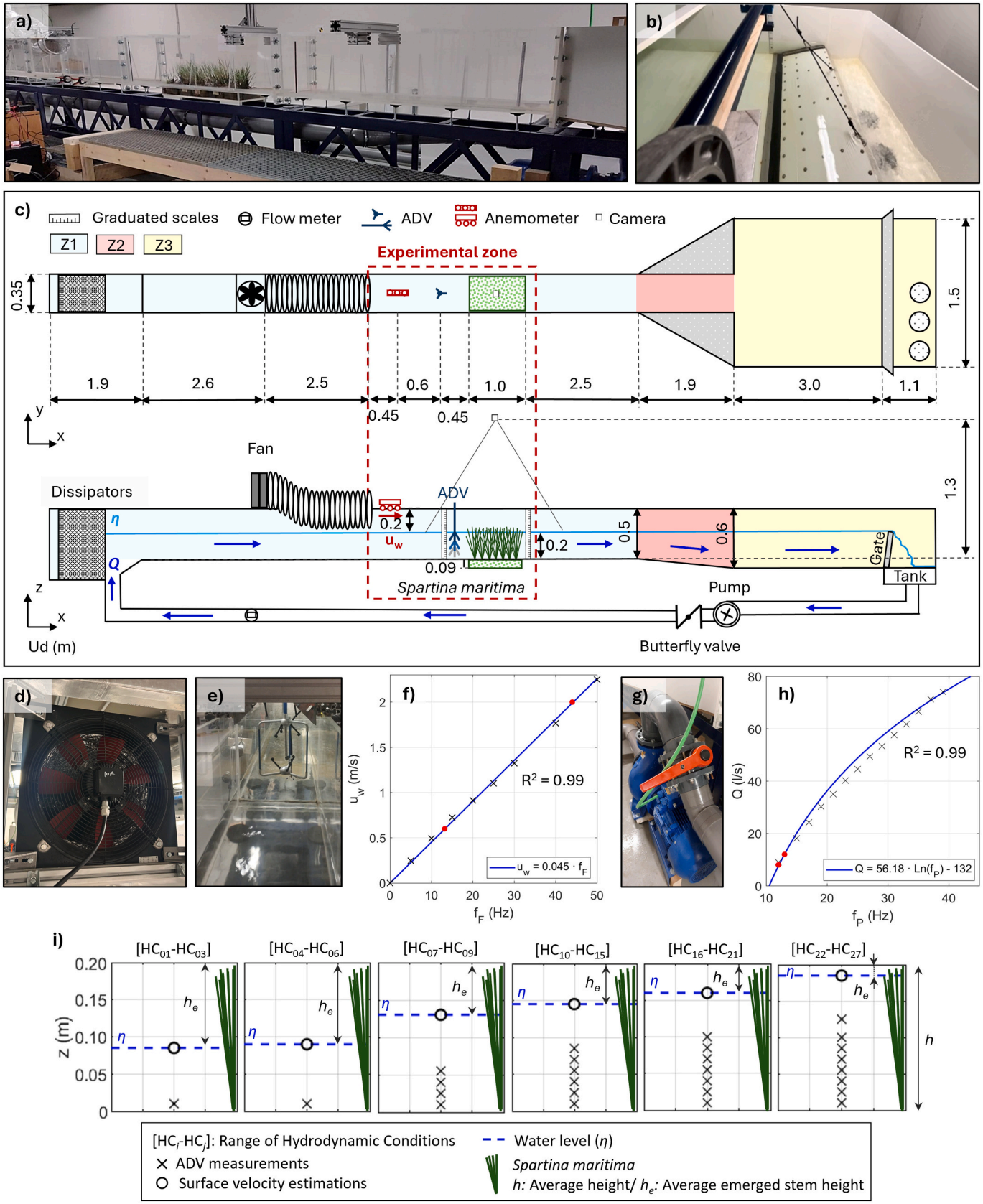

Fig. 1. Sketch of the experiments: a) an overview of the hydraulic flume; b) discharge gate; c) experimental set-up with flow meter, Acoustic Doppler Velocimeters (ADV), anemometer, and camera; d) fan; e) anemometer; f) fan performance curve: fan frequency (f_F) vs. wind speed (u_w); g) pump with butterfly valve; h) pump performance curve: pump frequency (f_P) vs. flow rate (Q). The red dots on the performance curves correspond to the hydrodynamic and wind conditions (HC) selected for analysis when the valve is open; and i) velocity measurement points and average emerged stem height (h_e) for the different HC. (For interpretation of the references to colour in this figure legend, the reader is referred to the web version of this article).

Table 1
Hydrodynamic conditions (HC) reproduced during the experiments, combining water levels (η), flow rates (Q), and wind speeds (u_w). The Q from HC_{01} to HC_{06} were obtained by valve throttling.

HC	η (m)	Q (m^3/s)	u_w (m/s)
01	0.085	0.0043	0.0
02			0.6
03			2.0
04	0.090	0.0043	0.0
05			0.6
06			2.0
07	0.130	0.0080	0.0
08			0.6
09			2.0
10	0.145	0.0080	0.0
11			0.6
12			2.0
13		0.0120	0.0
14			0.6
15			2.0
16	0.160	0.0080	0.0
17			0.6
18			2.0
19		0.0120	0.0
20			0.6
21			2.0
22	0.185	0.0080	0.0
23			0.6
24			2.0
25		0.0120	0.0
26			0.6
27			2.0

height of 1.3 m above the bottom of the flume. Finally, wind speed was recorded with an anemometer at a sampling rate of 10 Hz (Fig. 1e).

2.2. *Spartina maritima*

The *Spartina maritima* used in the experiments was collected at the low intertidal zone in the Marshes of Victoria, Santoña, and Joyel (northern Spain, within the Bay of Biscay), between −0.2 and 0.5 m with respect to the local zero (Fig. 2a). A total of four field surveys (FS) were conducted: two in the fall, on November 20, 2023 (FS_1) and December 19, 2023 (FS_2); one in the winter, on January 15, 2024 (FS_3); and one in the summer, on July 19, 2024 (FS_4).

A total of 10 trays (dimensions 26 × 19 × 9 cm) of vegetation were collected during each FS. The average height (h) of *Spartina maritima* was approximately 20 cm, which is a typical value for this species in the sampled area. Five of these trays were used in the experiments, while the remaining five were kept as spare in case the experimental procedures damaged the vegetation. These trays were maintained for a period of three weeks, as the vegetation showed no observable degradation when removed from its natural environment for this period. Fig. 2b shows five of the trays corresponding to FS_1, arranged according to the experimental design.

For characterization purposes, the volumetric density (ρ_v), defined as the effective volume occupied by the vegetation (V_V) divided by the total volume of its envelope (V_E), was estimated for each tray of *Spartina maritima* in the laboratory. To estimate V_V, a cubic container with an edge of 35 cm, filled with water to a height of 28.5 cm, and a graduated millimeter scale was used. The water volume displaced by each tray of *Spartina maritima* with sediment and the volume displaced by only the tray with sediment were measured inside this container. The difference between the two volumes provides V_V. V_E was estimated geometrically by assuming a parallelepiped shape and measuring the corresponding dimensions using graduated scales with millimeter accuracy.

Fig. 2d illustrates the ρ_v distributions of *Spartina maritima*, estimated using this method, for all field surveys. The distributions are shown as box plots. It is observed that the distributions from FS_1 to FS_3 were similar, with a median volumetric density ($\overline{\rho}_v$) between 6.2% and 7.4%, respectively, and standard deviations (σ) of 1%, without considering outliers. With these densities, trapping tests were performed under the hydrodynamic conditions from HC_{07} to HC_{27} defined in Table 1. However, the distribution associated with FS_4 exhibited significantly lower densities ($\overline{\rho}_v$ of 5.6%) and higher dispersion (σ = 2%). Fig. 2c shows the *Spartina* trays collected in FS_4. These densities were used for experiments related to hydrodynamic conditions from HC_{01} to HC_{03} (Fig. 2e-f). Finally, it was decided to test the effect of a potential increase in ρ_v on trapping. To this end, after the previous experiments were completed, the density of five of the vegetation trays, collected during FS_4, was artificially increased using the remaining vegetation available (hereafter, FS_4* refers to the artificial density modification of vegetation trays from FS_4). As a result of the replanting, the distribution associated with FS_4* was obtained ($\overline{\rho}_v$ = 8.7%, σ = 1.8%). With these ρ_v conditions, the trapping of plastic debris was analyzed under conditions from HC_{04} to HC_{06}.

Accordingly, three types of mean vegetation densities are described, namely: $\overline{\rho}_{v1}$ = 6.8%, associated with the combined distribution $FS_{1,2,3}$; $\overline{\rho}_{v2}$ = 5.6%, associated with FS_4; and $\overline{\rho}_{v3}$ = 8.7%, associated with FS_4*, for the subsequent analysis of the trapping results.

2.3. *Plastic materials*

The plastic debris under study corresponds to some of the most common plastic materials found in the marine environment in general and in salt marshes in particular. They are mostly macro- and mesoplastics of different shapes made of high-density polyethylene (HDPE), low-density polyethylene (LDPE), polypropylene (PP), and polystyrene (PS) (Zhang, 2017; Mazarrasa et al., 2019; Yao et al., 2019; Cozzolino et al., 2020; Cesarini and Scalici, 2022). In addition, the study of facemasks was included as their use has increased in recent years due to the global COVID-19 pandemic (Mourgkogiannis et al., 2018; De-la-Torre and Aragaw, 2021). The facemasks are manufactured from meltblown (MB) and spunbond (SB) nonwovens, which are mainly made of PP. Different shapes of macro- and mesoplastic were considered because although these are the sizes most prone to trapping, the shape of the debris will also be a determining factor. In order to eliminate variability from weathered field debris and isolate the effect of *Spartina maritima*, pristine plastic materials were used.

In total, the behavior of nine (9) types of plastic debris (P*i*) was evaluated (Fig. 3). Table 2 lists the main characteristics of these macro- and mesodebris, indicating aspects such as their density range ($\Delta\rho_P$), dimensions (a: major axis, b: intermediate axis, c: minor axis, and t: thickness), and shape defined by the Corey shape factor ($csf = c/\sqrt{a \cdot b}$, Corey, 1949). The csf is a non-dimensional parameter that describes particle shape, with 0 representing flat elements and 1 representing perfect spheres. In addition, each P*i* is defined by an average dimension, the equivalent nominal diameter (D_n), calculated using the equation derived from Francalanci et al. (2021): $D_n = a \cdot csf^{0.34} \cdot (b/a)^{0.5}$, which incorporates both particle size and shape. This approach was intended to explore if a single parameter could capture the combined effects of size and shape in trapping.

Material density ranges were obtained from manufacturer information when available and from the literature (Zhang, 2017). Specifically, the densities of P8 and P9 facemasks were obtained from the study of Bandi (2020). Dimensions were estimated by measuring 10 samples of each piece of plastic debris. The size of the plastic debris was measured using millimeter precision scales and a caliper with a resolution of 0.05 mm. In some cases, t was obtained from the manufacturer's information. Moreover, csf was used in this study to categorize P*i* based on their geometric shape. Plastic materials with csf close to 0, such as P5, P8, and P9, were classified as flat objects. Those with csf between 0 and 0.3 were considered elongated, typically resembling narrow cylinders with a dominant vertical axis (P6 and P7). Plastic debris with csf in the

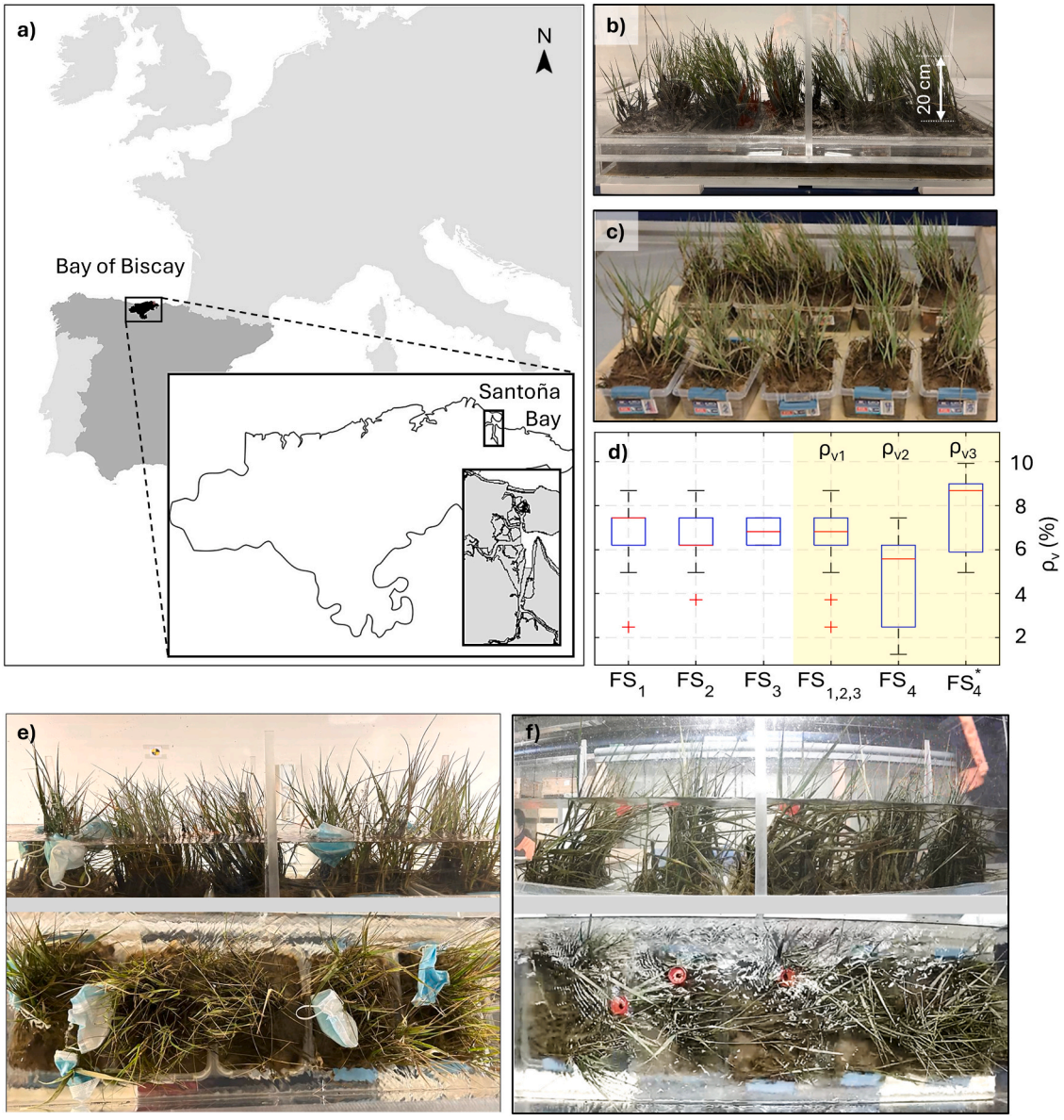

Fig. 2. Sampling of *Spartina maritima*: a) location of the Marshes of Victoria, Santoña, and Joyel (Spain); b) five trays of *Spartina maritima* in the hydraulic flume (corresponding to FS_1); c) 10 trays of *Spartina* collected during FS_4; d) box plots of *Spartina maritima* density from field surveys FS_1, FS_2, FS_3, and FS_4, from combined data $FS_{1,2,3}$, and from replanting densities FS_4*. Medians are represented by red lines, maximum and minimum values by black lines, and first and third quartiles by blue boxes. Red crosses represent outliers. Each distribution from the field surveys consists of 10 densities, while the replanting result consists of five. The distributions selected to describe the subsequent analysis of the trapping results are highlighted in yellow; and e-f) some of the plastic debris under study trapped in the vegetation trays from FS_4. (For interpretation of the references to colour in this figure legend, the reader is referred to the web version of this article).

0.3–0.5 range were identified as flattened cylinders with horizontal dimensions exceeding the vertical axis (P1 and P2). Finally, for *csf* between 0.5 and 0.8, the objects resemble more equilateral cylinders with comparable base and height (P3 and P4).

2.4. Experimental methodology

The trapping of each P*i* by *Spartina maritima* was tested individually in the flume for each HC defined in Table 1. The experiments were performed in three phases. In the first phase, the hydrodynamic and wind conditions were measured with the instrumentation described in subsection 2.1. In the second phase, the surface velocities were estimated (after removing the instrumentation and keeping only the camera). In the third phase, the plastic debris trapping was analyzed without the measuring instruments to avoid singularities that could affect the results.

Surface velocity is a relevant parameter in this study because buoyant plastic debris was analyzed. However, it cannot be determined directly with the ADV due to the inherent limitations of the instrument, which restricts measurements to approximately 5 cm below its location. Therefore, an experimental approach was used to estimate surface velocities. For this purpose, the trajectories of plastic elements, identical in composition to P5 (LDPE with a density of 910 kg/m^3) but with smaller dimensions of 5 mm × 5 mm × 0.07 mm, were analyzed inside the flume. These elements can be considered as flow tracers since they are characterized by Stokes numbers <0.03 ($St \ll 1$) for the evaluated HC. Twenty elements were released one by one at a distance of 60 cm before the beginning of the vegetated area, and their trajectories within the experimental area were subsequently monitored by the camera. The surface velocity was then derived from the analysis of the trajectories in the vicinity of the ADV location based on the method proposed by Passalacqua et al. (2023). This result was verified by the measurements

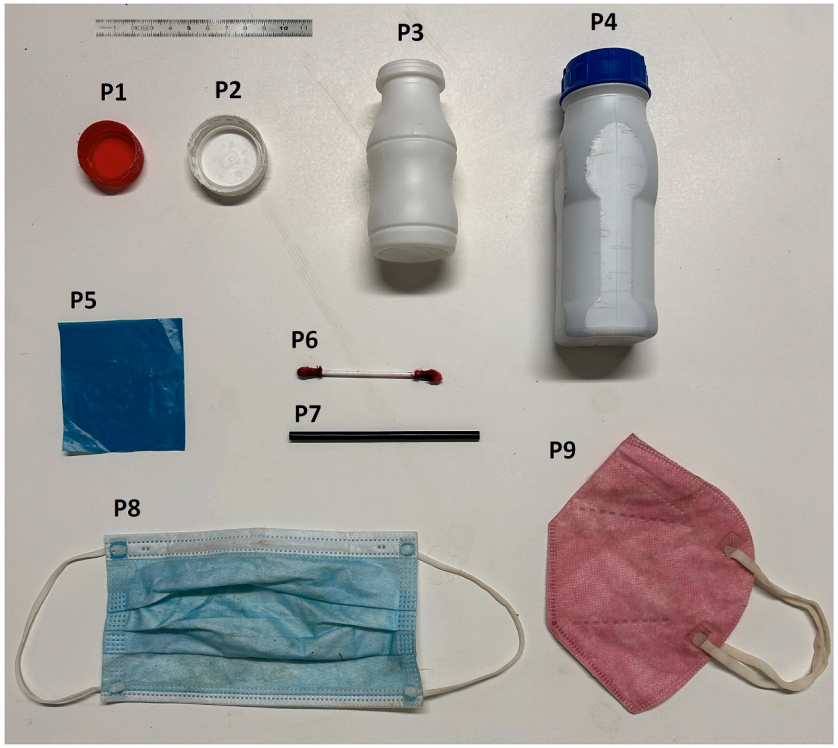

Fig. 3. Plastic materials (P*i*) under study.

Table 2
Main characteristics of the experimental plastic materials (P*i*): density range ($\Delta\rho_P$), longest axis (*a*), intermediate axis (*b*), smallest axis (*c*), thickness (*t*), Corey shape factor (*csf*), equivalent nominal diameter (D_n), and class defined according to D_n and *csf*.

Plastic debris type		Plastic material	$\Delta\rho_P$ (kg/m^3)	*a* (mm)	*b* (mm)	*c* (mm)	*t* (mm)	*csf* (−)	D_n (mm)	Class (size/shape)
P1	Bottle cap	HDPE	930–970	30	30	11	0.85	0.37	21	Meso/Flattened cylinder
P2	Bottle cap	HDPE	930–970	40	40	11	0.95	0.28	26	Macro/Flattened cylinder
P3	Bottle	HDPE	930–970	92	35	35	0.6	0.62	48	Macro/Equilateral cylinder
P4	Bottle	HDPE	930–970	130	48	48	0.95	0.61	67	Macro/Equilateral cylinder
P5	Piece of bag	LDPE	910–940	50	50	0.07	0.07	0.001	5	Meso/Flat
P6	Cotton swab	PP	850–950	73	3	3	1.0	0.20	9	Meso/Elongated cylinder
P7	Straw	PP	850–950	108	3	3	0.2	0.17	10	Meso/Elongated cylinder
P8	Surgical mask	MB&SB (PP)	350–410	175	95	1.5	1.5	0.01	28	Macro/Flat
P9	FFP2 mask	MB&SB (PP)	450	155	105	2.5	2.5	0.02	34	Macro/Flat

of the ADVs at depth, which allowed for the reconstruction and analysis of the velocity profile in the flume.

As for the trapping experiments, they were conducted for each of the 27 HC and the nine P*i*, resulting in a total of 243 experiments. Each experiment was carried out by releasing plastic debris at the end of the air duct in groups of five, without mixing different types. The number of items trapped by the vegetation within 40 s of release was then counted. In instances where the plastic made contact with the contour before reaching the vegetation, the data was excluded from the analysis. Ten valid replicates of each experiment were considered to assess the variability and consistency of trapping efficiency under controlled hydrodynamic and wind conditions, resulting in a total of 2430 releases. Lastly, it should be noted that these experiments were conducted in freshwater with a density of 1000 kg/m^3 and a water temperature of 15°C.

2.5. Data processing

The measurements, provided by the ADV at different depths ($u(z)$) and by the anemometer (u_w), were subjected to a filtering process to remove any potential noise from the original recorded series. This was achieved by using a percentile analysis to identify and remove outliers, thus ensuring the reliability of the data.

Surface velocity (u_s) was determined using video processing techniques, following the method proposed by Passalacqua et al. (2023). A MATLAB code-based algorithm was used to track plastic tracers and measure their travel time over a 1 m distance. The process involved: 1) extracting individual frames from the video, 2) converting pixel coordinates into physical coordinates to obtain real-world measurements, 3) enhancing tracer visibility by transforming RGB images into binary images, 4) identifying plastic tracer positions using blob analysis, 5) tracking tracer positions across successive frames to reconstruct their movement, and 6) calculating the velocity based on the displacement over time. This methodology enabled a quantitative analysis of plastic tracer movement and surface velocity estimation.

Velocity profiles were derived by fitting the average velocities from the ADVs and the average of the surface velocity estimates to water depth. The velocity profile in an open flume can be expressed as a logarithmic profile (French, 1985; van Rijn, 1990; González et al., 1996; Kirkgöz and Ardiçlioğlu, 1997):

$$u(z) = \frac{u_*}{\kappa} ln\left(\frac{z}{z_0}\right) \quad (1)$$

Table 3
Key variables for evaluating buoyant plastic debris trapping.

Physical factors	Variable	Description	Dimension	Unit	Obtention method
Flow & Wind	Flow rate, Q	Flow rate into the flume.	L^3T^{-1}	m^3/s	Flow meter
	Water level, η	Water surface height relative to the flume bottom.	L	m	Graduated scale.
	Wind velocity, u_w	Wind speed, which can directly or indirectly (by changing u_s) affect trapping.	LT^{-1}	m/s	Anemometer.
	Surface water velocity, u_s	Water velocity in the surface layer that transports buoyant debris.	LT^{-1}	m/s	Video analysis of plastic tracers (Passalacqua et al., 2023): $u_s = f_1(Q, \eta, u_w)$.
Vegetation	Effective volume of vegetation, V_V	Effective volume of vegetation cover.	L^3	m^3	Laboratory estimations based on water displacement.
	Envelope volume of vegetation, V_E	Enveloping volume of vegetation cover.	L^3	m^3	Laboratory estimations based on geometric approximations
	Average stem density, $\overline{\rho}_v$	Average volumetric ratio of V_V to V_E.	–	- (or %)	$\overline{\rho}_v = V_V/V_E$
	Average stem height, h	Average height of vegetation stems.	L	m	Graduated scale.
	Average emerged stem height, h_e	Average height of vegetation stems above the water surface.	L	m	$h_e = h - \eta$
Plastic debris	Major, Middle, Minor Axes, (a, b, c)	Measurement of debris size, representing the three principal dimensions.	L	m	Graduated scale and caliper.
	Corey shape factor, csf	Measurement of debris shape, indicating how closely the object approximates a sphere.	–	–	$csf = c/\sqrt{a \cdot b}$ (Corey, 1949).
	Equivalent nominal diameter, D_n	Characteristic debris size.	L	m	$D_n = a \cdot csf^{0.34} \cdot (b/a)^{0.5}$ (Francalanci et al., 2021).
Trapping	Trapping rate, T	Percentage of plastic debris retained by vegetation.	–	- (or %)	Direct count of trapped plastic debris.

where: u_* is the friction velocity, κ is the von Kármán constant (≈0.41), and z_0 is the bed roughness (≈ 0.001 for a smooth bottom).

Near the surface, wind can accelerate the flow due to an additional drag (Oost, 1991). To estimate this phenomenon, the flow velocity is accelerated by the following function, $\hat{c} \cdot (z/\hat{h})^{\hat{\beta}}$, where $\hat{h}$ is the total water depth; and $\hat{c}$ and $\hat{\beta}$ are parameters that control the intensity and shape of the wind effect above a critical depth (z_{crit}), respectively:

$$u(z) = \frac{u_*}{\kappa} ln\left(\frac{z}{z_0}\right), if z < z_{crit}$$
$$u(z) = \frac{u_*}{\kappa} ln\left(\frac{z}{z_0}\right) + \hat{c}\left(\frac{z}{\hat{h}}\right)^{\hat{\beta}}, if z \geq z_{crit} \quad (2)$$

The parameters u_*, z_{crit}, $\hat{c}$, and $\hat{\beta}$ were obtained by fitting the model function to the observed data using the nonlinear least squares method (Virtanen et al., 2020).

Finally, trapped items were counted at the end of each replicate in each experiment. Trapping rates (T) were obtained as the percentage of items trapped across all replicates relative to the total number of items released, which was 50 (i.e., 5 items/replicate per 10 replicates).

2.6. Dimensional analysis

Trapping buoyant plastic debris by estuarine vegetation is a complex phenomenon influenced by the interaction of several physical factors. These factors can be grouped into three main categories: hydrodynamic conditions, vegetation characteristics, and plastic debris properties (Table 3). In this study, a dimensional analysis was performed to identify the functional dependence between all these factors. Thus, the trapping rate (T) can be expressed as a function of:

$$T = f(Q, \eta, u_w, \overline{\rho}_v, h, a, b, c) \quad (3)$$

The water surface velocity (u_s), which influences the trapping of buoyant debris, can be expressed as a function of hydrodynamic and wind variables:

$$u_s = f_1(Q, \eta, u_w) \quad (4)$$

Vegetation characteristics relevant to buoyant debris trapping include density ($\overline{\rho}_v$) and emerged height (h_e). Vegetation density can be defined as a function of some physical properties of vegetation. Specifically, this study relates the effective volume of vegetation (V_V) to the enveloping volume of vegetation cover (V_E) to determine density:

$$\overline{\rho}_v = f_2(V_V, V_E) \quad (5)$$

while the emerged height is related to the average height of vegetation stems (h) and free surface elevation (η):

$$h_e = f_3(h, \eta) \quad (6)$$

For entrapment to occur, the emerged height must be greater than zero: $h_e > 0$.

Plastic debris can be characterized by dimensionless parameters that relate its three axes (a,b,c) to define its shape (csf) and characteristic size (D_n):

$$csf = f_4(a, b, c) \quad (7)$$

$$D_n = f_5(a, b, c) \quad (8)$$

As a result, it is expected that the plastic debris trapping rate (T) can be expressed as a function of the following variables:

$$T = f\left(u_s, \overline{\rho}_v, h_e, csf, D_n\right) \quad (9)$$

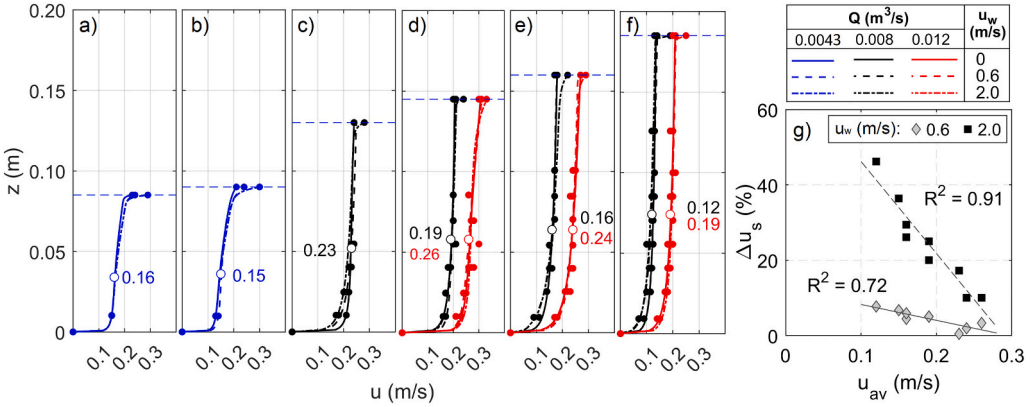

Fig. 4. Velocity profiles for each HC: a) $HC_{01–03}$, b) $HC_{04–06}$, c) $HC_{07–09}$, d) $HC_{10–15}$, e) $HC_{16–21}$, f) $HC_{22–27}$, with R^2 always >0.95 and the average flow velocity (u_{av}) represented by white filled circles; g) wind-induced changes in surface velocity (Δu_s) over the u_{av}.

3. Results

3.1. Hydrodynamic conditions in the flume

Panels "a" to "f" of Fig. 4 depict the velocity profiles obtained in the flume for each HC, where the average flow velocity (u_{av}) is defined as the velocity developed at a distance from the bottom equal to 40% of the total water depth (Te Chow, 1959; French, 1985). It is observed that the resulting profiles exhibited a high degree of similarity for the different combinations of flow rates and water levels, with the wind-induced effects only noticeable in the near-surface region. As verified in panels "c", "d", "e", and "f", for a given flow rate, the current velocity decreased as the water level increased, thereby resulting in an increase in the cross-sectional area. For instance, an increase in water level from 13 cm to 18.5 cm for a flow rate of 0.008 m^3/s resulted in a decrease in u_{av} from 0.23 m/s to 0.12 m/s. Similarly, panels "d", "e", and "f" show that an increase in flow rate for a given flume section resulted in an increase in flow velocity. As illustrated in panel "f", an increase in flow rate from 0.008 m^3/s to 0.012 m^3/s at a water level of 18.5 cm was associated with an increase in u_{av} from 0.12 m/s to 0.19 m/s.

In the velocity profiles, it is also observed that an increase in wind speed led to a proportional increase in the surface velocity. This phenomenon is clearly illustrated in panel "g" of Fig. 4, which shows the increase in surface velocity due to wind over the average velocity of each HC. Furthermore, it is evidenced that the wind-induced effect on the surface velocity was more relevant for the combinations of water level and flow rate that correspond to lower average flow velocities. This is since, in systems with low hydrodynamic velocities, wind can constitute a relevant proportion of the total energy. However, in the case of strong currents, the influence of wind becomes negligible in comparison to the energy of the current. To illustrate this, a comparison between the hydrodynamic conditions defined by the lowest ($HC_{22–24}$: u_{av}=0.12 m/s) and highest ($HC_{13–15}$: u_{av}=0.26 m/s) flow velocities demonstrated that, for the same wind intensity, the most significant changes in surface velocity with respect to the calm wind condition occurred in $HC_{22–24}$. In these cases, wind speeds of 0.6 m/s and 2 m/s resulted in surface velocity increases of 8% and 46%, respectively, while in $HC_{13–15}$, these values were 3% and 10%, respectively.

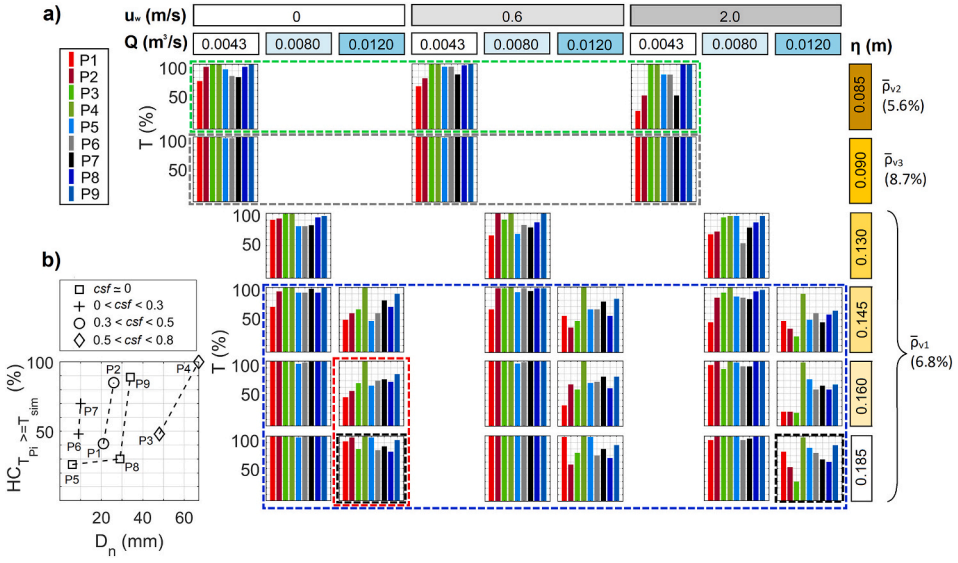

Fig. 5. Trapping efficiency (T) of *Spartina maritima*: a) bar charts accounting for different vegetation densities ($\bar{\rho}_v$), different plastic types (Pi), and hydrodynamic/wind conditions (HC: η, Q, u_w). Note that the red, green, blue, and gray shades represent plastic types with similar shapes, namely: flattened cylinders like bottle caps (P1 and P2), equilateral cylinders like bottles (P3 and P4), elongated elements (P6 and P7), and flat elements (P5, P8 and P9), respectively. b) Percentage of HC where T of each Pi (T_{Pi}) equals or exceeds T of similarly shaped materials (T_{sim}). (For interpretation of the references to colour in this figure legend, the reader is referred to the web version of this article).

3.2. Trapping rates of buoyant macro- and mesoplastic debris

3.2.1. Overview of experimental results

The set of experimental results obtained is summarized in Fig. 5. Fig. 5a shows the bar charts of the trapping rates of *Spartina maritima*, characterized by different mean volumetric densities ($\bar{\rho}_v$), for the different types of plastic debris (P*i*) and hydrodynamic (η, Q) and wind (u_w) conditions analyzed (Table 1 and Table 2).

For the lowest vegetation coverage ($\bar{\rho}_{v2}$=5.6%, green dashed box in Fig. 5), the greatest wind-induced variation in T was exhibited by smaller, flattened cylindrical plastic items such as bottle caps (P1 and P2). Under calm wind conditions (u_w=0), T reached 74% and 96% for P1 and P2, respectively. However, for the strongest wind (u_w=2 m/s), these values decreased by approximately 45%. In contrast, elongated items (P6 and P7) exhibited high trapping rates (exceeding 80%) at wind speeds of <0.6 m/s, with only slight reductions (approximately 20% or less) observed at u_w values of 2 m/s. Larger items, such as bottles (P3 and P4) or flat debris (P5, P8, and P9), demonstrated consistent trapping rates of approximately 100%, regardless of wind conditions.

As the mean vegetation density increases to 8.7% ($\bar{\rho}_{v3}$, gray dashed box in Fig. 5), an overall larger T is observed for all plastic types, regardless of hydrodynamic or wind conditions, suggesting a positive correlation between vegetation density and trapping.

For an intermediate *Spartina* density ($\bar{\rho}_{v1}$=6.8%), a more complex interaction between trapping, hydrodynamic forces, wind conditions, and plastic properties can be inferred due to the greater amount of related data collected during the experiments. In general, higher water levels were found to increase trapping rates for a given flow rate and wind speed, i.e., higher T are associated with lower surface velocities. As an example, at the highest flow rate (0.012 m^3/s) during calm wind conditions, a 2.5 cm rise in water level (from 16.0 to 18.5 cm) resulted in a nearly 50%, a 36%, and a 15% increase in trapping for P1, P5, and P3, respectively (red dashed box in Fig. 5). Analogously, when water level and wind speed were held constant, a reduction in flow rate resulted in an increase in T. As noted above, these conditions also correspond to lower surface velocities. For instance, at the three highest water levels (14.5, 16, and 18.5 cm) and across all wind conditions analyzed, P6 exhibited an approximately 30% greater values in trapping efficiency at a flow rate of 0.008 m^3/s compared to a flow rate of 0.012 m^3/s (blue dashed box in Fig. 5). Moreover, trapping efficiency generally decreased as wind speed increased when flow rates and water levels remained constant. This could be a direct result of wind drag or wind-induced surface currents. As highlighted in the black dashed boxes in Fig. 5, for a flow rate of 0.012 m^3/s and a water level of 18.5 cm, when comparing the calm wind with the highest wind speed of 2 m/s, the absolute reduction in T for all P*i* ($i = 1, 2, \ldots, 9$) ranged from 2% to 50%, depending on the plastic type.

Furthermore, the bar graphs confirm that T is also dependent on the size and shape of plastic debris. Fig. 5b represents the percentage of hydrodynamic and wind conditions in which the trapping rate of each P*i* exceeds or matches that of similarly shaped materials: flat items ($csf \cong 0$; P5, P8, P9); elongated items ($0<csf<0.3$; P6, P7); bottle caps ($0.3<csf<0.5$; P1, P2); and bottles ($0.5<csf<0.8$; P3, P4). Across all categories, larger items consistently showed higher trapping rates. For instance, P9 exceeded or equaled the trapping rates of P5 and P8 in nearly 90% of the conditions analyzed. In the same way, P7 outperformed or equaled P6 in 70% of cases, P2 surpassed or equaled P1 in 85% of the conditions, and P4 consistently exhibited a trapping rate greater than or equal to P3 across all conditions analyzed.

Considering these results, it can be concluded that the trapping rates of buoyant plastic debris are closely related to several different factors identified in subsection 2.6, including surface current velocities, wind speeds, intrinsic properties of the plastic debris itself, such as shape and size, and vegetation characteristics, such as its volumetric density. Moreover, a factor not directly mentioned, but related to water level, is the height of emerging stems. A comprehensive analysis of the effect of plastic debris characteristics, wind speed, emerged stem height on trapping rates is presented below, not in isolation, but considering the wide range of hydrodynamic conditions and vegetation densities under study.

3.2.2. Influence of surface velocity, plastic debris size and shape on trapping rates

Fig. 6a depicts the scatter plots, where the white, gray, and black dots denote calm, moderate, and stronger wind conditions, respectively. Additionally, Fig. 6a shows the curve fit of T over u_s for each type of P*i* for the average density of *Spartina maritima* ($\bar{\rho}_{v1}$). As shown in this panel, there was no clear influence of wind on trapping. However, it is observed that the trapping measurements fit well with a shifted power law as a function of surface velocity, indicating a strong correlation

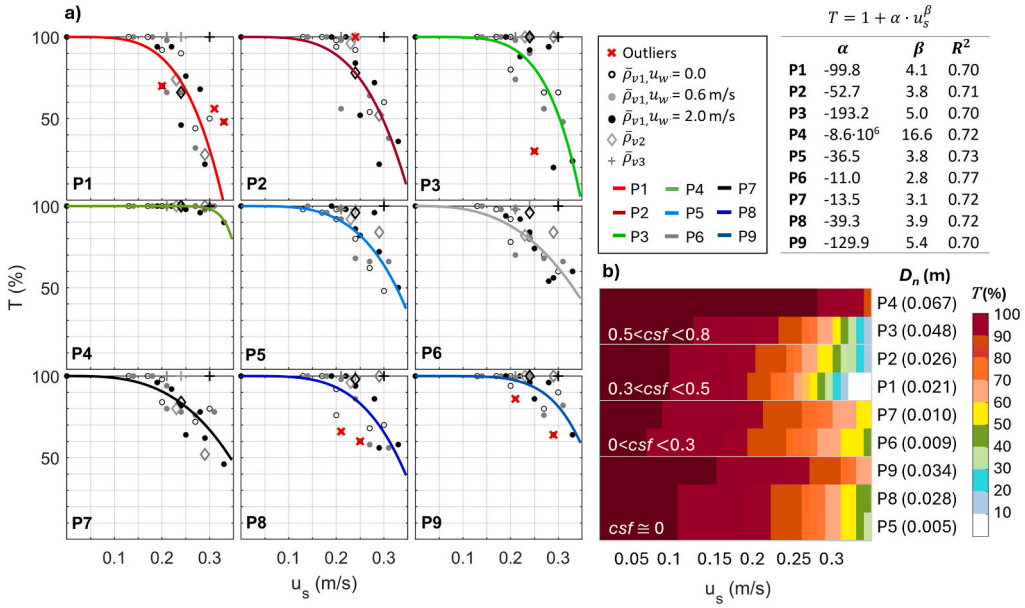

Fig. 6. Trapping rate (T) as a function of surface velocity (u_s): a) Scatter plots and curve fits between T and u_s for each P*i* and b) Curve-fit matrix of T and u_s organized by the shapes (csf) and sizes (D_n) of each P*i*.

between the two variables (R^2 value of at least 0.7). The coefficients "α" and "β", and thus the trapping, were found to depend on both the shape and size of the plastic debris. Furthermore, the trapping data associated with $\bar{\rho}_{v2}$ (white diamonds) and $\bar{\rho}_{v3}$ (black crosses) are superimposed in Fig. 6a, showing that the discrepancies in behavior were only significantly different when the density of the vegetation was artificially increased to $\bar{\rho}_{v3}$, where the analyzed plastic types were trapped regardless of the value of u_s.

Fig. 6b shows these results organized by the shape (*csf*) and size (D_n) of the plastic debris under investigation. Notwithstanding the interdependence of D_n and *csf*, the individual assessment of their effects offered a more precise representation of trapping behavior. In general, surface velocities below 0.10 ± 0.02 m/s resulted in trapping rates exceeding 90%. In contrast, velocities around 0.22 ± 0.02 m/s facilitated the release of more plastic elements, with trapping rates between 80% and 90%. Finally, velocities of 0.32 ± 0.01 m/s led to the release of up to 50% of the items. In particular, an analysis of the shape of the plastic debris indicates that *Spartina maritima* was particularly effective for trapping flat or elongated elements (*csf*<0.3). At the highest surface velocity of 0.33 m/s, at least 40% of this debris was trapped. Conversely, three-dimensional elements (*csf*>0.3) showed a limited capacity to be trapped, with <10% of the items remaining trapped at the same velocity. The only exception is the largest material evaluated, P4, which demonstrated 90% entrapment even at these high velocities. In terms of the dimensions of the plastic debris, it is demonstrated that the larger the debris, the greater the probability of it being trapped. This observation is consistent across all categories of debris representative of their shape.

Based on these results, it can be concluded that the trapping rate of plastic debris by *Spartina maritima* is strongly related to surface velocity, which in turn depends on current and wind conditions, as well as the shape and size of the debris.

3.2.3. *Influence of wind speed on trapping rates*

Fig. 7 provides more detailed information on the influence of wind speed on trapping. Panels "a$_i$" illustrate the trapping rate of each plastic type under the hydrodynamic and wind conditions analyzed (Table 1 and Table 2). Each panel represents a set of three HC with constant flow rates and water levels, varying only the wind speed, thus showing the influence of wind speed on *T* for that flow condition. Panels "b$_i$" show the statistical distributions of *T* for all P*i* in the form of box plots.

Overall, it can be observed that higher wind speeds were associated with lower trapping efficiencies. Panels "a1-b1" refer to HC associated with the lowest vegetation density ($\bar{\rho}_{v2}$=5.6%), while panels "a2-b2" refer to the highest vegetation density ($\bar{\rho}_{v3}$=8.7%). This explains the significant differences in trapping rates despite similar average HC (u_{av}<0.15 m/s). Thus, while $\bar{\rho}_{v2}$ allowed small elongated (P6 and P7) and flattened cylindrical (P1 and P2) materials to escape, especially at higher wind speeds, $\bar{\rho}_{v3}$ trapped all P*i* regardless of wind speed.

For the remaining panels, $\bar{\rho}_{v1}$ is 6.8%. As a result, the trapping efficiency for the three wind speeds can be directly compared under similar average flow conditions. The shaded boxes classify HC according to average flow velocities that generate similar trapping behaviors: blue, green, and red shades represent velocities below 0.15 m/s, between 0.15 and 0.20 m/s, and above 0.20 m/s, respectively. The highest trapping rates, about 100% for all P*i*, were observed at the lowest flow velocities (panels "a6-b6" and "a8-b8"), and only the highest wind speed of 2 m/s managed to release some of these elements. Intermediate flow velocities (panels "a3-b3", "a4-b4", and "a9-b9") resulted in lower *T*, and even lower trapping occurred at higher flow velocities (panels "a5-b5" and "a7-b7"). On average under calm wind conditions, 6% to 8% of the items escaped at intermediate flow velocities, while 32% to 34% escaped at higher flow velocities. As wind speed increased, more elements escaped: for instance, at the highest wind speed analyzed (2 m/s), an average of 14% to 26% of the items escaped at moderate flow velocities, and up to 50% escaped for higher flow velocities. These findings thus confirm that, in addition to plastic debris characteristics, vegetation density, and hydrodynamics, wind conditions influence the trapping efficiency of the buoyant plastic debris analyzed here by *Spartina* vegetation. However, it remains unclear whether this influence is direct, as wind drags, or indirect, as surface currents.

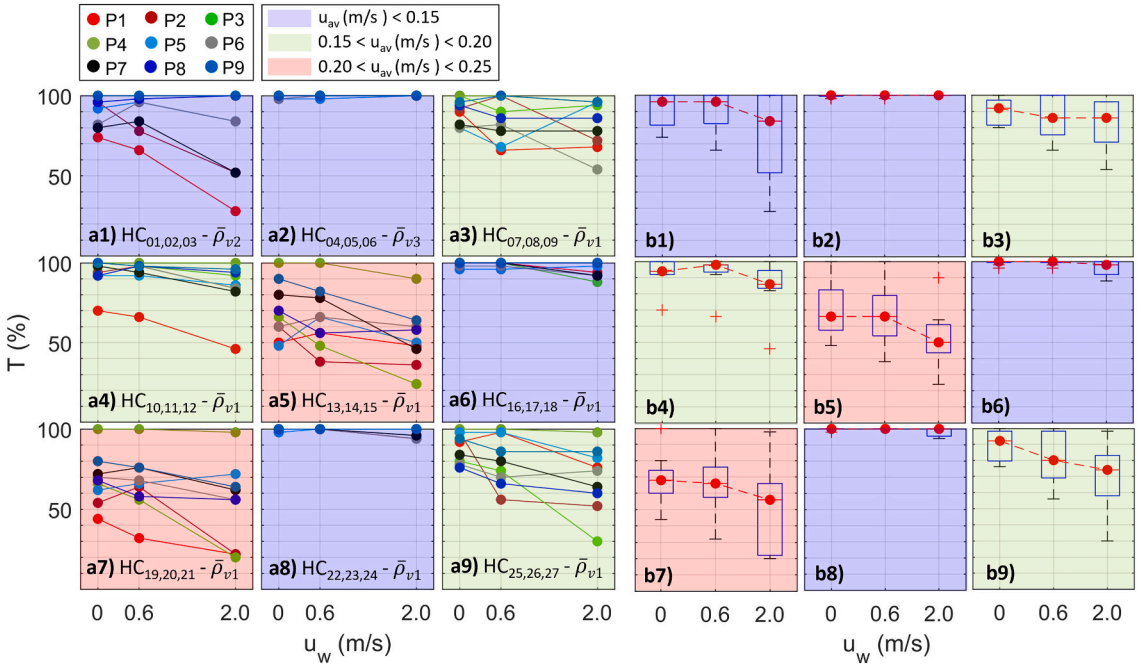

Fig. 7. Trapping rate (*T*) as a function of wind speed (u_w): a) For each plastic type (P*i*), where HC corresponds to the conditions in Table 1 and $\bar{\rho}_v$ to the vegetation densities studied; and b) Statistical distributions (box plots) considering all P*i*, where the median (red dots), maximum and minimum (black lines), first and third quartiles (blue boxes), and outliers (red crosses) are reported. Note that the blue, green, and red shades represent different categories of mean flow velocities (u_{av}), with velocities below 0.15 m/s, between 0.15 and 0.20 m/s, and above 0.20 m/s, respectively. (For interpretation of the references to colour in this figure legend, the reader is referred to the web version of this article).

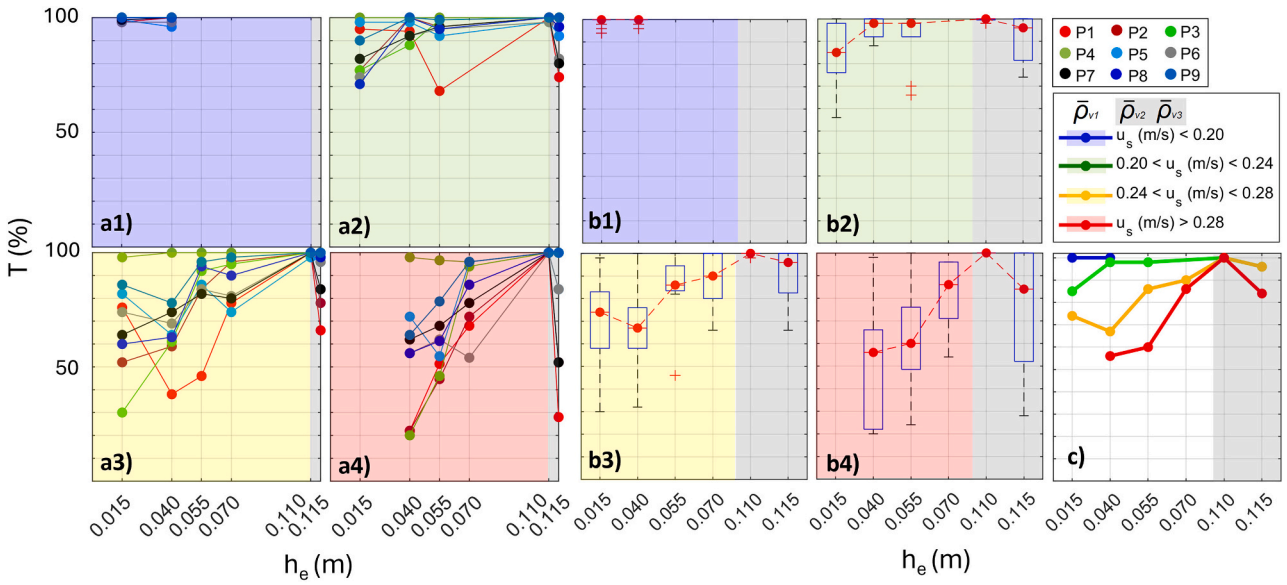

Fig. 8. Trapping rate (T) as a function of the emerged height of vegetation (h_e): a) For each plastic type (P*i*); and b) Statistical distributions (box plots) considering all P*i*, where the median (red dots), maximum and minimum (black lines), first and third quartiles (blue boxes), and outliers (red crosses) are reported. Note that the blue, green, yellow, and red shades represent different categories of surface velocities (u_s) for the mean vegetation density $\bar{\rho}_{v1}$, while the shaded gray areas correspond to $\bar{\rho}_{v2}$ and $\bar{\rho}_{v3}$. (For interpretation of the references to colour in this figure legend, the reader is referred to the web version of this article).

3.2.4. *Influence of emerged stem height on trapping rates*

In order to analyze the effect of the emerged stem height (h_e) on the trapping rate, the hydrodynamic and wind conditions were classified into four categories based on surface velocity. The class represented in panels "a1-b1" (u_s<0.2 m/s) encompasses five HC. The category shown in panels "a2-b2" (0.2<u_s<0.24 m/s) includes seven HC. The category of panels "a3-b3" (0.24<u_s<0.28 m/s) consists of eight HC, and the category in panels "a4-b4" (u_s >0.28 m/s) comprises seven HC. This classification was required to generate comparable trapping behavior across different h_e values, given the direct correlation between emerged height and water levels, which can result in varying expected behaviors. Thus, it is expected that greater vegetation emerged height will result in higher T, but also in lower water levels and, therefore, higher flow velocities, which may release trapped debris. Accordingly, the average trapping rate versus h_e is shown in Fig. 8 for each HC category and plastic type. Note that the colored shades represent the different u_s categories for the mean vegetation density $\bar{\rho}_{v1}$, while the shaded gray areas correspond to $\bar{\rho}_{v2}$ and $\bar{\rho}_{v3}$.

An important verification in this figure is the relevant role of vegetation density. A h_e of 11 cm corresponded to $\bar{\rho}_{v2}$ (8.7%), which blocked almost all P*i* in all four surface velocity classes. Conversely, a h_e of 11.5 cm, although similar in magnitude, was associated with $\bar{\rho}_{v3}$ (5.6%) and allowed plastic debris, primarily the smallest flattened cylindrical (P1 and P2) and elongated (P6 and P7) materials, to escape. Considering all P*i*, an average of 4% of the items escaped (with a maximum of 30% for P1) when u_s was below 0.28 m/s, and 16% escaped when u_s exceeded this threshold (with a maximum of 72% for P1).

For the remaining emerged heights, associated with $\bar{\rho}_{v1}$ (6.8%), it can generally be inferred that for a given surface velocity range, a larger emerged height resulted in higher trapping efficiency. However, as illustrated in panel "c", the surface velocity remained the dominant factor, with lower surface velocity consistently leading to higher trapping efficiency. It is important to note that the influence of surface velocity was especially relevant at lower emerged heights. In this sense, for a h_e of 4 cm, the average trapping rate ranged from 56% to 100% for u_s >0.28 m/s and u_s below 0.2 m/s, respectively. However, as emerged height increases, the effect of surface velocity diminishes. Thus, for a h_e of 7 cm, the observed variation in trapping ranged from 86% to 100%. These results demonstrate that the emerged stem height also has a notable impact on the trapping rate. Nevertheless, it can be stated that the surface velocity remains the dominant factor for the plastic types and HC under analysis.

3.3. *Trapping model of buoyant macro- and mesoplastic debris for Spartina maritima*

In light of the findings detailed in subsection 3.2, it can be inferred that the trapping of buoyant macro- and mesoplastic debris by *Spartina maritima* fundamentally depends on the following key factors: surface velocity (resulting here from hydrodynamic and wind conditions), plastic debris characteristics (shape and size), and estuarine vegetation (volumetric density and emerged stem height). This section describes a trapping model (*T-model*) of buoyant macro- and mesoplastics derived from the aforementioned variables and the density of vegetation sampled in the marshes (Fig. 9a).

The *T-model* shows that the surface velocity is always a parameter that influences the trapping rate, while the importance of the plastic debris size depends on its shape. In this regard, the greater the three-dimensional geometry of debris (i.e., the higher the *csf*), the more its size affects trapping.

For purposes of comparison, Fig. 9b illustrates the model-predicted trapping for 16 hypothetical macro- and mesoplastic types, classified into four shape categories and four nominal sizes (D_{n1} =0.01 m, D_{n2}=0.02 m, D_{n3}=0.05 m, and D_{n4}=0.10 m). For flat debris (*csf* ≅0), the probability of trapping depends almost exclusively on the surface velocity, regardless of size. For instance, velocities of 0.27 and 0.34 m/s are associated with trapping rates of 80% and 50%, respectively. For elongated debris (0<*csf*<0.3), smaller elements with D_{n1} behave like flat debris, achieving 80% and 50% trapping rates for surface velocities of 0.25 and 0.34 m/s, respectively. However, debris size also begins to have an effect, with the two largest elongated materials (D_{n3-4}) being more susceptible to trapping even at surface velocities above 0.3 m/s. For the three-dimensional flattened debris (0.3<*csf*<0.5), the influence of size is even more relevant. The probability of *Spartina maritima* trapping small plastic debris (D_{n1-2}) with this shape is 80% and 50% for velocities near 0.19 and 0.27 m/s, respectively. The two largest debris items (D_{n3-4}) require velocities of 0.26 and 0.31 m/s to achieve the same trapping rates, respectively. Finally, three-dimensional debris with

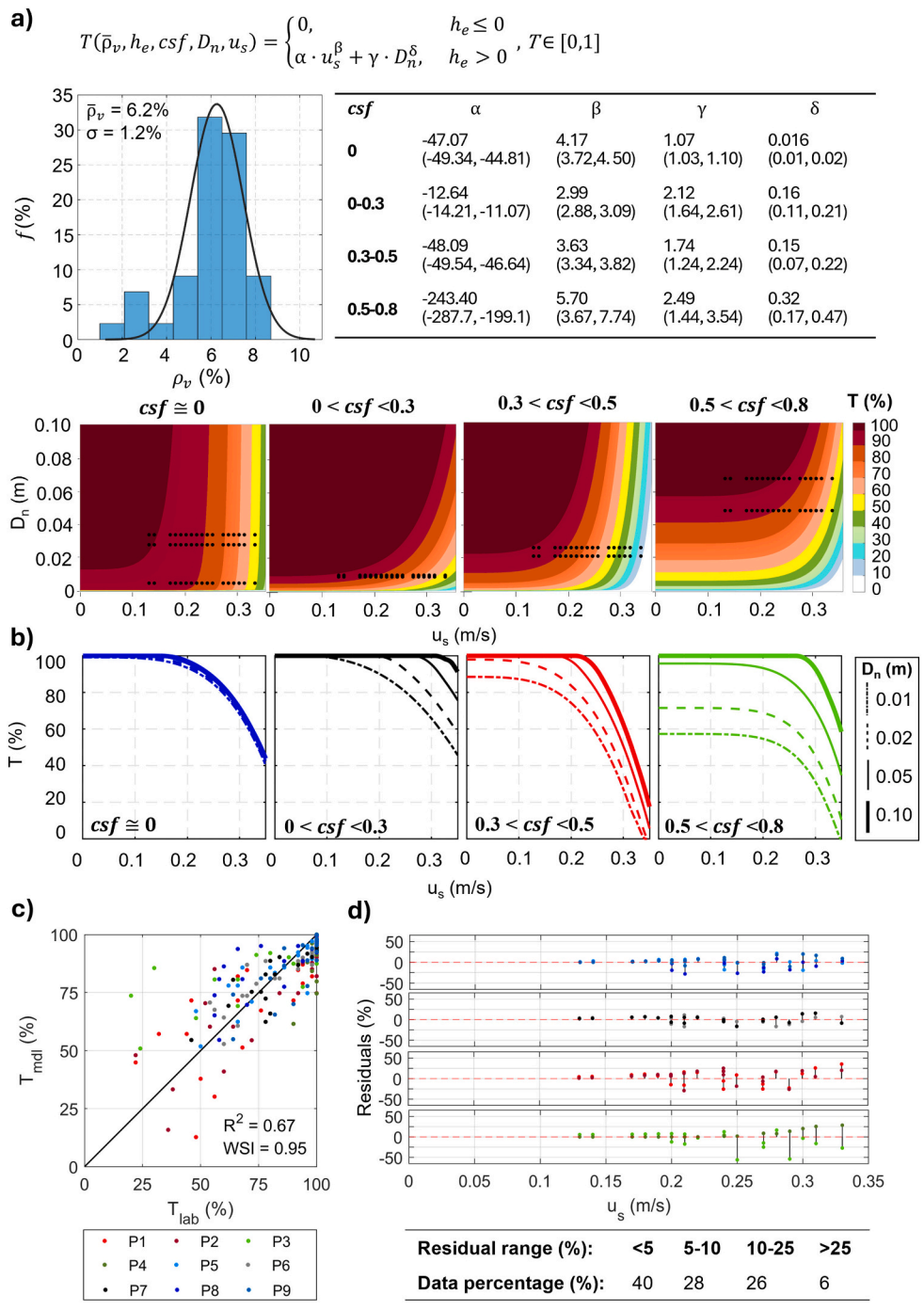

Fig. 9. a) Trapping model (*T-model*) of buoyant macro- and mesoplastics by *Spartina maritima* as a function of vegetation properties ($\bar{\rho}_v$= 6.2%, h_e), plastic debris characteristics: shape (*csf*) and size (D_n), and surface flow velocity (u_s). The probability density function of ρ_v, for which the *T-model* was obtained, results from combining data sets from field surveys without considering densities from artificial replanting; b) some results of the *T-model* for plastic debris within different shape categories and D_n; c) Scatter plot between trapping rates from the laboratory (T_{lab}) and the model (T_{mdl}); and d) *T-model* residuals (T_{lab}- T_{mdl}) over u_s.

comparable dimensions (0.5<*csf*<0.8) exhibit an enhanced effect of size on trapping. It is observed that the maximum trapping efficiency for small debris (D_{n1-2}) reaches only 60% to 70% even at the lowest velocities, and decreases to 50% when surface velocities reach about 0.26 m/s. In contrast, larger debris (D_{n3-4}) exhibited a higher trapping rate. At velocities close to 0.30 m/s, 80% of the debris is trapped, while at velocities close to 0.34 m/s, the trapping rate is 50%. In conclusion, these results suggest that larger plastic debris requires higher surface velocities to avoid trapping, while debris shape influences the balance between surface velocity and debris size in determining trapping efficiency. However, the limited size range of plastic samples analyzed in this study constrains a comprehensive assessment of size effects. Therefore, these size-related results should be interpreted with caution and require further validation through studies examining a wider range of plastic debris sizes.

Fig. 9c depicts the scatter plot of the trapping rates derived from laboratory data and those predicted by the model. The coefficient of determination (R^2) between both data sets is 0.67, and the Wilmott Skill Index (*WSI*) (Willmott, 1981) is 0.95. These statistical indicators collectively suggest that, in general terms, the model is performing well

with regard to trapping rates. Nevertheless, as illustrated in panel "d", the model also exhibits some significant residual values in certain predictions. In general, only 6% of the residuals show discrepancies exceeding 25%, and 1% (i.e., two predictions) is near 50%. These discrepancies are within the shape category of equilateral cylinders (bottles).

4. Discussion

The efficiency of the estuarine vegetation *Spartina maritima* to trap macro- and mesoplastic debris commonly found in salt marshes was evaluated using physical modeling. A series of hydrodynamic conditions characteristic of salt marshes were simulated in a hydraulic flume by varying water levels, currents, and wind intensities. A range of water levels was evaluated that allowed *Spartina maritima* stems to emerge between 40% and 90% of their total height (approximately 20 cm). Fluctuations in flow velocity typically range from 0.05 to 0.30 m/s during tidal cycles in salt marshes (Monge-Ganuzas et al., 2017). To match these conditions, the experiments examined velocities in the same range for the specified water levels, achieving mean velocities between 0.12 and 0.26 m/s, with surface velocities reaching up to 0.33 m/s due to wind (Fig. 4).

The trapping capacity of *Spartina maritima* stems was evaluated for three densities: one from field sampling during the fall-winter period, with an average volumetric coverage of 6.8%; another from sampling during the summer period, with an average coverage of 5.6%; and one from artificial replanting, with a coverage of 8.7% (Fig. 2d). The difference in densities between the fall-winter and summer seasons can be attributed to the fact that the optimal growth of this vegetal species requires constant humidity, moderate salinity, and low sulfide concentrations. Surface runoff was the only freshwater input to the salt marshes where *Spartina maritima* was sampled. Therefore, a reduction in freshwater inputs during the summer months could result in alterations in substrate salinity, while elevated temperatures could increase sulfide concentrations. Both factors may negatively affect stem density (Adams and Bate, 1995; Sánchez et al., 1997). The life cycle of *Spartina maritima* plays an important role in the dynamics and processes of estuarine ecosystems. Periods of increased stem density enhance sedimentation processes (Neumeier and Ciavola, 2004; Wilkie et al., 2012) and contribute to the trapping of plastic debris in its vegetative structures (Gallitelli et al., 2023).

As for the types of plastic debris, several buoyant macro- and mesoplastics with nominal diameters ranging from 5 mm to 67 mm were analyzed to complete and extend the types analyzed in previous experimental studies. These studies focused mainly on buoyant and non-buoyant microplastics (de Los Santos et al., 2021; Ogbuagu et al., 2022), but also on non-buoyant mesoplastics (Gallitelli et al., 2023). The plastic materials under study exhibited a variety of shapes, such as bottle caps, bottles, cotton swabs, straws, plastic bag fragments and facemasks, as the shape of the debris, in conjunction with its size, plays a significant role in determining its potential for becoming trapped.

The results of the experiments indicate that generalized trapping rates exceed 90% when the surface velocity is <0.2 m/s (Fig. 6). Although velocities below 0.2 m/s are highly probable in salt marshes, previous field studies have demonstrated that lower concentrations of plastic debris are observed in low marshes, where *Spartina* spp. develop, compared to high marshes where other community types such as *Juncus* spp. or *Halimione* spp. are present (Mazarrasa et al., 2019; Yao et al., 2019). The discrepancy between the experimental results and those observed in the field can be primarily attributed to the experimental setup, which consistently directs the plastic debris towards the vegetation, where it may or may not become trapped. Under estuarine conditions, however, the hydrodynamics transporting plastic debris may or may not drive it towards vegetation, reducing the probability of entrapment. For instance, in the marshes where vegetation was collected for these experiments, *Spartina maritima* was found at depths between −0.2 and 0.5 m from local zero. Considering an average height of 20 cm for this vegetation and the annual frequency of flooding by only astronomical tides, the probability of plastic reaching each *Spartina maritima* plant is estimated to be about 6%. This reduction factor adjusts the experimental trapping probability to an estimate closer to field observations. Thus, the combination of a 6% probability of plastic arrival and a 90% probability of trapping provided by the experiments would result in an effective trapping of 4.5% when the surface velocity is <0.2 m/s.

Based on these experimental results, a model of macro- and mesoplastic trapping by *Spartina maritima* was developed (*T-model* in Fig. 9). The model was identified as an effective preliminary tool, demonstrating promising performance in predicting the trapping of plastic debris in *Spartina maritima* low marshes, particularly during the fall-winter season, but also during the summer. As new data from ad hoc experiments are incorporated, the model has the potential to be further refined and improved. The *T-model* can be integrated into numerical models of plastic debris transport and dispersion, similar to the approach taken with the "*beaching*" parameter in particle models such as TrackMPD, Delft3D-PART, or TESEO, among others (e.g., Jalón-Rojas et al., 2019; Núñez et al., 2019, 2021). The *T-model* dynamically estimates trapping based on local hydrodynamics (u_s), plastic debris characteristics (D_n, csf), and vegetation properties ($\bar{\rho}_v$, h_e). In a Lagrangian tracking model, these parameters can be incorporated as follows: At each time step, the model reads the velocity fields that transport particles with predefined size and shape, either as fixed values or drawn from statistical distributions. Vegetation density and emerged height can be included as constant values or as spatially and temporally variable data. When a particle enters a vegetated area, the *T-model* calculates the trapping probability based on these variables, determining whether the particle is retained or continues its trajectory. As a result, the data provided by numerical models would be improved, allowing managers and policymakers to better formulate effective strategies and policies to clean up and mitigate plastic pollution.

Although the trapping model provides valuable insight into plastic debris trapping under controlled experimental conditions, it is important to recognize that it may not fully capture the complexity of natural estuarine dynamics. Further research, including new laboratory, field, and numerical studies, is needed to complete and expand the database generated in this study and to make the *T-model* more robust. Due to the complexity of the issue and the multitude of variables involved, several factors related to transport drivers, plastic debris properties, vegetation characteristics, or parametrizations would benefit from more detailed investigation.

In terms of hydrodynamics, it would be interesting to investigate not only constant water levels, but also the effect of the tidal cycle on trapping, as this is a relevant factor in tidal estuaries. Tidal flow in natural salt marshes is bidirectional, with the landward phase playing an important role in debris accumulation. Incorporating full tidal cycle studies could provide a more comprehensive understanding of debris dynamics and improve the assessment of trapping efficiency. With regard to wind, a more comprehensive investigation of the direct effect of wind drag on the trapping rates of plastic debris of different shapes, sizes and densities would be a valuable contribution to the existing body of research. New experiments could be designed in a reservoir without currents to evaluate how wind, in isolation, influences the transport and trapping of plastic debris as a function of its buoyancy and exposed surface area.

Another valuable area of investigation would be the impact of vegetation density. To comprehensively assess its influence on plastic trapping, future research should explore a wider range of naturally occurring densities across diverse hydrodynamic conditions. This should encompass seasonal fluctuations and consider *Spartina* spp., *Halimione* spp., and *Juncus* spp., extending beyond the limited range examined in this study.

As far as the characteristics of plastic debris are concerned, it is worth continuing to investigate new shapes, sizes, and densities beyond those

examined here and in previous studies, as this would allow for a more comprehensive understanding of plastic debris behavior (de Los Santos et al., 2021; Ogbuagu et al., 2022; Gallitelli et al., 2023; Kerpen et al., 2024). For instance, expanded polystyrene (EPS) foam, a prevalent type of plastic debris in estuarine environments, would be a pertinent material to study. This material was not included in the study due to its unique fragmentation characteristics, which result in a wide variability of shapes and sizes, requiring dedicated experiments. Moreover, as these experiments conducted in the present study were in freshwater, it is important to note that increased salinity in estuarine or marine environments could also affect the buoyancy of some debris types, potentially modifying trapping rates. Similarly, factors such as biofouling can also affect the buoyancy of plastic debris over time and therefore the dynamics of trapping (Jalón-Rojas et al., 2022; Núñez et al., 2023a).

Regarding parametrization, effective parameter selection is important for accurately quantifying plastic debris trapping. In this study, hydrodynamics is represented by the water surface velocity (u_s), which indirectly accounts for wind effects (u_w); vegetation is characterized by its density ($\bar{\rho}_v$) and height, specifically the emerged stem height (h_e); and plastic debris is described by the equivalent nominal diameter (D_n), as defined by Francalanci et al. (2021), and the Corey shape factor (*csf*). Although these last two parameters are not completely independent, both were included in the analysis because the initial approach was to examine the individual and combined effects of size and shape on plastic debris trapping. However, the experimental results indicated that analyzing these effects separately provided a better description of the trapping behavior. Given the strong correlation observed between D_n and $(a{\cdot}b{\cdot}c)^{1/3}$ for the plastic materials analyzed, its use as a representative measure of size in our analysis is validated. Structuring the problem in terms of these key physical parameters provides a systematic framework for analyzing trapping behavior across different experimental and field conditions, facilitating comparisons and guiding future refinements of the model.

Finally, to evaluate the effectiveness of the trapping model and ensure its general applicability, it would be interesting to compare the validity of the model derived from experiments with data from drift surveys or field data collected in estuaries (e.g., Wilkie et al., 2012; Mazarrasa et al., 2019; Yao et al., 2019; Cozzolino et al., 2020; Almeida et al., 2023; Girones et al., 2024). This comparison can be conducted through numerical assessments in different estuaries with a notable presence of vegetation that are influenced by different drivers, such as tidal, river, wind, salinity, or temperature fluxes.

5. Conclusions

The results of this study extend the findings of previous research on plastic debris trapping in vegetated estuarine zones, incorporating new types of vegetation, plastic types, and hydrodynamic conditions. A further novel contribution is the enhanced understanding of the correlation between trapping rates and a range of factors associated with plastic debris, vegetation, and hydrodynamic characteristics. The findings suggest that *Spartina maritima* acts as a natural trap, with lower surface velocities, higher stem densities and emerged heights, as well as larger sizes and flatter shapes of plastic debris favoring trapping. Furthermore, it was identified that, for a density of *Spartina maritima* comparable to that observed in the marshes during the fall-winter period, the dominance of surface velocity or plastic debris size in trapping primarily depends on the shape of the debris. Thus, the surface velocity is more significant for flat elements (e.g., pieces of bags or facemasks), while size plays a more relevant role for three-dimensional elements, such as bottles.

In addition, a simple model (*T-model*) was developed that relates the above variables to trapping rates. This trapping model can be integrated into numerical models of plastic debris transport and dispersion, thereby enhancing their predictive capacity and providing valuable information to managers and policymakers in the development of effective strategies against marine plastic pollution in estuaries. The incorporation of new data from further experimental, numerical or field research to complement the information provided here will allow the trapping model to be improved and refined.

CRediT authorship contribution statement

Paula Núñez: Writing – review & editing, Writing – original draft, Visualization, Validation, Supervision, Resources, Methodology, Investigation, Formal analysis, Data curation, Conceptualization. **Laura Pérez-García:** Writing – review & editing, Investigation, Conceptualization. **Seyed Meysam Rezaee:** Writing – review & editing, Investigation, Conceptualization. **Javier F. Bárcena:** Writing – review & editing, Supervision, Project administration, Methodology, Funding acquisition, Conceptualization. **Andrés García:** Writing – review & editing, Supervision, Project administration, Methodology, Funding acquisition, Conceptualization.

Declaration of Generative AI and AI-assisted technologies in the writing process

During the preparation of this work the authors used *DeepL Write* in order to improve the readability and language of the manuscript. After using this tool, the authors reviewed and edited the content as needed and take full responsibility for the content of the published article.

Declaration of competing interest

The authors declare that they have no known competing financial interests or personal relationships that could have appeared to influence the work reported in this paper.

Acknowledgments

The authors acknowledge the support of the Programa de Ciencias Marinas (PCM), funded by the Ministry of Science and Innovation of the Spanish Government and the Regional Governments of Andalucía, Baleares, Canarias, Cantabria, Comunidad Valenciana, Galicia, and Murcia (PRTR-C17·I1). This program, part of the ThinkInAzul I + D + i Complementary Plan, has provided essential funding for this research, in line with the 2030 Agenda for Sustainable Development and the Decade of the Oceans initiative. Moreover, this research was also partially funded by PID2021-127358NB-I00-MICIU/AEI/10.13039/501100011033 and by FEDER as a way of making Europe. Finally, we express our deep gratitude to Margot Sánchez for her invaluable support and dedication throughout the development of this work.

Data availability

Data will be made available on request.

References

Adams, J.B., Bate, G.C., 1995. Ecological implications of tolerance of salinity and inundation by Spartina maritima. Aquat. Bot. 52 (3), 183–191.
Almeida, C.M.R., Sáez-Zamacona, I., Silva, D.M., Rodrigues, S.M., Pereira, R., Ramos, S., 2023. The role of estuarine wetlands (saltmarshes) in sediment microplastics retention. Water 15 (7), 1382.
Alsina, J.M., Jongedijk, C.E., van Sebille, E., 2020. Laboratory measurements of the wave-induced motion of plastic particles: influence of wave period, plastic size and plastic density. J. Geophys. Res. Oceans 125 (12), e2020JC016294.
Bandi, M.M., 2020. Electrocharged facepiece respirator fabrics using common materials. Proceedings of the Royal Society A 476 (2243), 20200469.
Cesarini, G., Scalici, M., 2022. Riparian vegetation as a trap for plastic litter. Environ. Pollut. 292, 118410.
Chen, Z., Li, G., Bowen, M., Coco, G., 2023. Retention of buoyant plastic in a well-mixed estuary due to tides, river discharge and winds. Mar. Pollut. Bull. 194, 115395.
Corey, A.T. (1949) Influence of shape on the fall velocity of sand grains.

Cózar, A., Echevarría, F., González-Gordillo, J.I., Irigoien, X., Úbeda, B., Hernández-León, S., Palma, Á.T., Navarro, S., García-de-Lomas, J., Ruiz, A. and others (2014) 'Plastic debris in the open ocean', Proc. Natl. Acad. Sci., 111(28), pp. 10239–10244.
Cozzolino, L., Nicastro, K.R., Zardi, G.I., de Los Santos, C.B., 2020. Species-specific plastic accumulation in the sediment and canopy of coastal vegetated habitats. Sci. Total Environ. 723, 138018.
Crawford, C.B., Quinn, B., 2017. Microplastics, standardisation and spatial distribution. Microplastic pollutants 5, 115–122.
de Los Santos, C.B., Krång, A.-S., Infantes, E., 2021. Microplastic retention by marine vegetated canopies: Simulations with seagrass meadows in a hydraulic flume. Environ. Pollut. 269, 116050.
De-la-Torre, G.E., Aragaw, T.A., 2021. What we need to know about PPE associated with the COVID-19 pandemic in the marine environment. Mar. Pollut. Bull. 163, 111879.
Díaz-Torres, E.R., Ortega-Ortiz, C.D., Silva-Iñiguez, L., Nene-Preciado, A., Orozco, E.T., 2017. Floating marine debris in waters of the Mexican Central Pacific. Mar. Pollut. Bull. 115 (1–2), 225–232.
Forsberg, P.L., Sous, D., Stocchino, A., Chemin, R., 2020. Behaviour of plastic litter in nearshore waters: First insights from wind and wave laboratory experiments. Mar. Pollut. Bull. 153, 111023.
Francalanci, S., Paris, E., Solari, L., 2021. On the prediction of settling velocity for plastic particles of different shapes. Environ. Pollut. 290, 118068.
French, R.H., 1985. Open-channel hydraulics. McGraw-Hill.
Galgani, F., Hanke, G., Maes, T., 2015. Global distribution, composition and abundance of marine litter. Marine anthropogenic litter 29–56.
Gallitelli, L., Di Lollo, G., Adduce, C., Maggi, M.R., Trombetta, B., Scalici, M., 2023. Aquatic plants entrap different size of plastics in indoor flume experiments. Sci. Total Environ. 863, 161051.
Galloway, T.S., Cole, M., Lewis, C., 2017. Interactions of microplastic debris throughout the marine ecosystem. Nature ecology & evolution 1 (5), 116.
García-Rellán, A., Ares, D.V., Brea, C.V., López, A.F., Bugallo, P.M.B., 2023. Sources, sinks and transformations of plastics in our oceans: review, management strategies and modelling. Sci. Total Environ. 854, 158745.
Girones, L., Adaro, M.E., Pozo, K., Baini, M., Panti, C., Fossi, M.C., Marcovecchio, J.E., Ronda, A.C., Arias, A.H., 2024. Spatial distribution and characteristics of plastic pollution in the salt marshes of Bahía Blanca estuary. Argentina', Science of The Total Environment 912, 169199.
González, J.A., Melching, C.S., Oberg, K.A., 1996. 'Analysis of Open-Channel Velocity Measurements Collected with an Acoustic Doppler Current Profiler', in *1st International Conference on New/Emerging Concepts for Rivers*. IWR Association, Chicago, USA.
Iuppa, C., Passalacqua, G., Faraci, C., 2024. An equilibrium criterion for plastic debris fate in wave-driven transport. Mar. Pollut. Bull. 206, 116758.
Jalón-Rojas, I., Wang, X.H., Fredj, E., 2019. A 3D numerical model to track marine plastic debris (TrackMPD): Sensitivity of microplastic trajectories and fates to particle dynamical properties and physical processes. Mar. Pollut. Bull. 141, 256–272.
Jalón-Rojas, I., Romero-Ramírez, A., Fauquembergue, K., Rossignol, L., Cachot, J., Sous, D., Morin, B., 2022. Effects of biofilms and particle physical properties on the rising and settling velocities of microplastic fibers and sheets. Environ. Sci. Technol. 56 (12), 8114–8123.
Kerpen, N.B., Schlurmann, T., Schendel, A., Gundlach, J., Marquard, D., Hüpgen, M., 2020. Wave-induced distribution of microplastic in the surf zone. Front. Mar. Sci. 7, 590565.
Kerpen, N.B., Larsen, B.E., Schlurmann, T., Paul, M., Guler, H.G., Goral, K.D., Carstensen, S., Christensen, E.D., Fuhrman, D.R., 2024. Microplastic retention in marine vegetation canopies under breaking irregular waves. Sci. Total Environ. 912, 169280.
Kirkgöz, M.S., Ardiçlioğlu, M., 1997. Velocity profiles of developing and developed open channel flow. J. Hydraul. Eng. 123 (12), 1099–1105.
Kühn, S., Van Franeker, J.A., 2020. Quantitative overview of marine debris ingested by marine megafauna. Mar. Pollut. Bull. 151, 110858.
Law, K.L., 2017. Plastics in the marine environment. Annu. Rev. Mar. Sci. 9 (1), 205–229.
Lebreton, L.C.M., Van Der Zwet, J., Damsteeg, J.W., Slat, B., Andrady, A., Reisser, J., 2017. River plastic emissions to the world's oceans. Nat. Commun. 8, 15611.
Lebreton, L.-M., Greer, S.D., Borrero, J.C., 2012. Numerical modelling of floating debris in the world's oceans. Mar. Pollut. Bull. 64 (3), 653–661.
Lechthaler, S., Waldschläger, K., Stauch, G., Schüttrumpf, H., 2020. The way of macroplastic through the environment. Environments 7 (10), 73.
Li, G., Chen, Z., Bowen, M., Coco, G., 2024. Transport and retention of sinking microplastics in a well-mixed estuary. Mar. Pollut. Bull. 203, 116417.
Liro, M., Emmerik, T., van, Wyżga, B., Liro, J., Mikuś, P., 2020. Macroplastic storage and remobilization in rivers. Water 12 (7), 2055.
López, A.G., Najjar, R.G., Friedrichs, M.A.M., Hickner, M.A., Wardrop, D.H., 2021. Estuaries as filters for riverine microplastics: Simulations in a large, coastal-plain estuary. Front. Mar. Sci. 8, 715924.
Maximenko, N., Hafner, J., Niiler, P., 2012. Pathways of marine debris derived from trajectories of Lagrangian drifters. Mar. Pollut. Bull. 65 (1–3), 51–62.
Mazarrasa, I., Puente, A., Núñez, P., García, A., Abascal, A.J., Juanes, J.A., 2019. Assessing the risk of marine litter accumulation in estuarine habitats. Mar. Pollut. Bull. 144, 117–128.
Mazarrasa, I., Neto, J.M., Bouma, T.J., Grandjean, T., Garcia-Orellana, J., Masqué, P., Recio, M., Serrano, Ó., Puente, A., Juanes, J.A., 2023. Drivers of variability in blue carbon stocks and burial rates across European estuarine habitats. Sci. Total Environ. 886, 163957.
Meijer, L.J.J., Van Emmerik, T., Van Der Ent, R., Schmidt, C., Lebreton, L., 2021. More than 1000 rivers account for 80% of global riverine plastic emissions into the ocean. Sci. Adv. 7 (18), eaaz5803.
Monge-Ganuzas, M., Gainza, J., Liria, P., Epelde, I., Uriarte, A., Garnier, R., González, M., Núñez, P., Jaramillo, C., Medina, R., 2017. Morphodynamic evolution of Laida beach (Oka estuary, Urdaibai biosphere reserve, southeastern Bay of Biscay) in response to supratidal beach nourishment actions. J. Sea Res. 130, 85–95.
Mourgkogiannis, N., Kalavrouziotis, I.K., Karapanagioti, H.K., 2018. Questionnaire-based survey to managers of 101 wastewater treatment plants in Greece confirms their potential as plastic marine litter sources. Mar. Pollut. Bull. 133, 822–827.
Nations, U. (2015) 'Transforming our world: the 2030 agenda for sustainable development', United Nations, New York, 1, p. 41.
Neumeier, U., Ciavola, P., 2004. Flow resistance and associated sedimentary processes in a Spartina maritima salt-marsh. J. Coast. Res. 20 (2), 435–447.
Newbould, R.A., Powell, D.M., Whelan, M.J., 2021. Macroplastic debris transfer in rivers: a travel distance approach. Frontiers in Water 3, 724596.
Núñez, P., García, A., Mazarrasa, I., Juanes, J.A., Abascal, A.J., Méndez, F., Castanedo, S., Medina, R., 2019. A methodology to assess the probability of marine litter accumulation in estuaries. Mar. Pollut. Bull. 144, 309–324.
Núñez, P., Castanedo, S., Medina, R., 2020. A global classification of astronomical tide asymmetry and periodicity using statistical and cluster analysis. J. Geophys. Res. Oceans 125 (8), e2020JC016143.
Núñez, P., Castanedo, S., Medina, R., 2021. Role of ocean tidal asymmetry and estuarine geometry in the fate of plastic debris from ocean sources within tidal estuaries. Estuar. Coast. Shelf Sci. 259, 107470.
Núñez, P., Misic, C., Cutroneo, L., Capello, M., Medina, R., Besio, G., 2023a. Biofilm-induced effect on the buoyancy of plastic debris: An experimental study. Mar. Pollut. Bull. 193, 115239.
Núñez, P., Romano, A., García-Alba, J., Besio, G., Medina, R., 2023b. Wave-induced cross-shore distribution of different densities, shapes, and sizes of plastic debris in coastal environments: A laboratory experiment. Mar. Pollut. Bull. 187, 114561.
Ogbuagu, C.C., Kassem, H., Udiba, U.U., Stead, J.L., Cundy, A.B., 2022. Role of saltmarsh systems in estuarine trapping of microplastics. Sci. Rep. 12 (1), 15546.
Oost, W.A., 1991. The wind profile in a wave flume. J. Wind Eng. Ind. Aerodyn. 37 (2), 113–121.
Passalacqua, G., Iuppa, C., Faraci, C., 2023. A simplified experimental method to estimate the transport of non-buoyant plastic particles due to waves by 2D image processing. J. Mar. Sci. Eng. 11 (8). https://doi.org/10.3390/jmse11081599.
Rech, S., Macaya-Caquilpán, V., Pantoja, J.F., Rivadeneira, M.M., Jofre Madariaga, D., Thiel, M., 2014. Rivers as a source of marine litter – a study from the SE Pacific. Mar. Pollut. Bull. 82 (1–2), 66–75.
Sánchez, J.M., Otero, X.L., Izco, J., Macías, F., 1997. Growth form and population density of Spartina maritima (Curtis) Fernald in Northwest Spain. Wetlands 17, 368–374.
Chow, V., Te, 1959. Open-Channel Hydraulics. McGraw-Hill, Classical Textbook Reissue.
Tiller, R., Arenas, F., Galdies, C., Leitão, F., Malej, A., Romera, B.M., Solidoro, C., Stojanov, R., Turk, V., Guerra, R., 2019. Who cares about ocean acidification in the Plasticene? Ocean & coastal management 174, 170–180.
Tramoy, R., Gasperi, J., Colasse, L., Silvestre, M., Dubois, P., Noûs, C. and Tassin, B. (2020) 'Transfer dynamics of macroplastics in estuaries–new insights from the Seine estuary: part 2. Short-term dynamics based on GPS-trackers', *Mar. Pollut. Bull.*, 160, p. 111566.
van Rijn, L.C., 1990. Principles of Fluid Flow and Surface Waves in Rivers, Estuaries, Seas, and Oceans. Aqua Publications, Oldemarkt.
Van Sebille, E., England, M.H., Froyland, G., 2012. Origin, dynamics and evolution of ocean garbage patches from observed surface drifters. Environ. Res. Lett. 7 (4), 44040.
Van Sebille, E., Aliani, S., Law, K.L., Maximenko, N., Alsina, J.M., Bagaev, A., Bergmann, M., Chapron, B., Chubarenko, I., Cózar, A., 2020. The physical oceanography of the transport of floating marine debris. Environ. Res. Lett. 15 (2), 23003.
Vermeiren, P., Muñoz, C.C., Ikejima, K., 2016. Sources and sinks of plastic debris in estuaries: A conceptual model integrating biological, physical and chemical distribution mechanisms. Mar. Pollut. Bull. 113 (1–2), 7–16.
Virtanen, P., Gommers, R., Oliphant, T.E., Haberland, M., Reddy, T., Cournapeau, D., Burovski, E., Peterson, P., Weckesser, W., Bright, J. and others (2020) 'SciPy 1.0: fundamental algorithms for scientific computing in Python', Nat. Methods, 17(3), pp. 261–272.
Wilkie, L., O'Hare, M.T., Davidson, I., Dudley, B., Paterson, D.M., 2012. Particle trapping and retention by Zostera noltii: a flume and field study. Aquat. Bot. 102, 15–22.
Willmott, C.J., 1981. On the validation of models. Phys. Geogr. 2 (2), 184–194.
Wu, F., Pennings, S.C., Tong, C., Xu, Y., 2020. Variation in microplastics composition at small spatial and temporal scales in a tidal flat of the Yangtze estuary. China', Science of The Total Environment 699, 134252.
Yao, W., Di, D., Wang, Z., Liao, Z., Huang, H., Mei, K., Dahlgren, R.A., Zhang, M., Shang, X., 2019. Micro-and macroplastic accumulation in a newly formed Spartina alterniflora colonized estuarine saltmarsh in Southeast China. Mar. Pollut. Bull. 149, 110636.
Zhang, H., 2017. Transport of microplastics in coastal seas. Estuar. Coast. Shelf Sci. 199, 74–86.
Zhao, S., Zhu, L., Li, D., 2015. Microplastic in three urban estuaries. China', *Environmental pollution* 206, 597–604.
Zhao, X., Niu, Z., Ma, Y., Zhang, Y., Li, Y., Zhang, R., 2024. Exploring the dynamics of antibiotic resistome on plastic debris traveling from the river to the sea along a representative estuary based on field sequential transfer incubations. Sci. Total Environ. 923, 171464.